PNAS RESEARCH ARTICLE | CHEMISTRY OPEN ACCESS

Chemical bond reorganization in intramolecular proton transfer revealed by ultrafast X-ray photoelectron spectroscopy

Yonghao Gu[a,b,1], Haiwang Yong[c,1], Bing Gu[d], and Shaul Mukamel[a,b,1]

Edited by Oleg Prezhdo, University of Southern California, Los Angeles, CA; received December 4, 2023; accepted March 21, 2024, by Editorial Board Member Peter J. Rossky

Time-resolved X-ray photoelectron spectroscopy (TR-XPS) is used in a simulation study to monitor the excited state intramolecular proton transfer between oxygen and nitrogen atoms in 2-(iminomethyl)phenol. Real-time monitoring of the chemical bond breaking and forming processes is obtained through the time evolution of excited-state chemical shifts. By employing individual atomic probes of the proton donor and acceptor atoms, we predict distinct signals with opposite chemical shifts of the donor and acceptor groups during proton transfer. Details of the ultrafast bond breaking and forming dynamics are revealed by extending the classical electron spectroscopy chemical analysis to real time. Through a comparison with simulated time-resolved photoelectron spectroscopy at the valence level, the distinct advantage of TR-XPS is demonstrated thanks to its atom specificity.

time-resolved X-ray photoelectron spectroscopy | intramolecular proton transfer | ultrafast science

The real-time monitoring of the atoms and molecules undergoing elementary chemical reaction events is a central goal of femtochemistry. Optical spectroscopies usually capture the delocalized features of the entire molecule rather than the chemical bond dynamics of individual atoms. In this theoretical study, we show that chemical shifts of atom-specific signals can directly reveal dynamics of the chemical bond breaking and forming.

Proton transfer is one of the most fundamental reactions in chemistry and biophysics (1, 2). The associated bond-breaking and forming between hydrogen and the donor and acceptor atoms make it a perfect target to study local dynamics (3, 4). Excited-state intramolecular proton transfer (ESIPT) is of wide interest with applications to sensors, light generations and photoswitching devices (5–11). Photoexcitation can change the electronegative character of the proton donor and acceptor groups in a molecule. The subsequent proton exchange through intramolecular hydrogen bonding is known as ESIPT. Traditionally, it has been probed by steady-state and time-resolved spectroscopies (12–18). However, since ultrafast ESIPT occurs on a femtosecond scale, direct observation of its dynamics including details of the donor and acceptor groups is still challenging. Advanced measurements with site-selectivity, sufficient temporal and spectral resolution are therefore called for. Entangled light photoelectron spectroscopy that combines both high energy and time resolutions has been recently investigated (19).

Advancements in ultrashort pulse technology have enabled the observation and modulation of elementary physical and chemical processes on their natural time scale. The generation of X-ray pulses in free-electron lasers (FELs) and high-order harmonic generation (HHG) sources has made it possible to study the ultrafast dynamics in molecular systems with core-level excitation and attosecond temporal resolutions (20–23). Time-resolved X-ray photoelectron spectroscopy (TR-XPS) is most suitable for monitoring ultrafast dynamics (24–33). Conventional steady-state XPS can obtain site-specific chemical shifts of static ground-state of molecules, leading to the classical electron spectroscopy chemical analysis (ESCA) technique (34). It can reveal the bonding pattern of atoms in different chemical species. TR-XPS can observe site-specific excited-state chemical shifts in real time, extending ESCA to the real-time evolution of chemical shifts providing local bonding dynamics of atoms in molecules. The atom specificity of this method stems from the localized nature of the core-level ionization. Generally, the core orbitals of the reaction center atoms are more sensitive to chemical bond changes in its vicinity compared to delocalized valence orbitals. The significant chemical shifts of core ionization make it possible to achieve high spectral resolution. Recent experiments have illustrated the capacity of TR-XPS to monitor local charge dynamics and photodissociation dynamics (35, 36).

Significance

Ultrashort X-ray free electron lasers provide opportunities to study the chemical reactions in real time by core-level excitation. In this theoretical study, we simulate the time-resolved X-ray photoelectron spectroscopy signals for probing an excited state intramolecular proton transfer process. The local bonding dynamics is monitored by time evolution of chemical shifts. Through separate observations of the core ionization of proton donor and acceptor atoms, we find that the donor atom generates a signal with rapid red shift while the acceptor atom yields an opposite blue shift. We show that these signatures cannot be obtained by photoelectron signals of valence levels. This technique thus provides a unique access to chemical bond breaking and forming events in ultrafast chemical processes.

Author contributions: Y.G., H.Y., and S.M. designed research; Y.G., H.Y., and B.G. performed research; Y.G., H.Y., and S.M. analyzed data; and Y.G., H.Y., B.G., and S.M. wrote the paper.

The authors declare no competing interest.

This article is a PNAS Direct Submission. O.P. is a guest editor invited by the Editorial Board.

[1]To whom correspondence may be addressed. Email: yonghaog@uci.edu, hyong@ucsd.edu, or smukamel@uci.edu.

This article contains supporting information online at https://www.pnas.org/lookup/suppl/doi:10.1073/pnas.2321343121/-/DCSupplemental.

Published April 18, 2024.

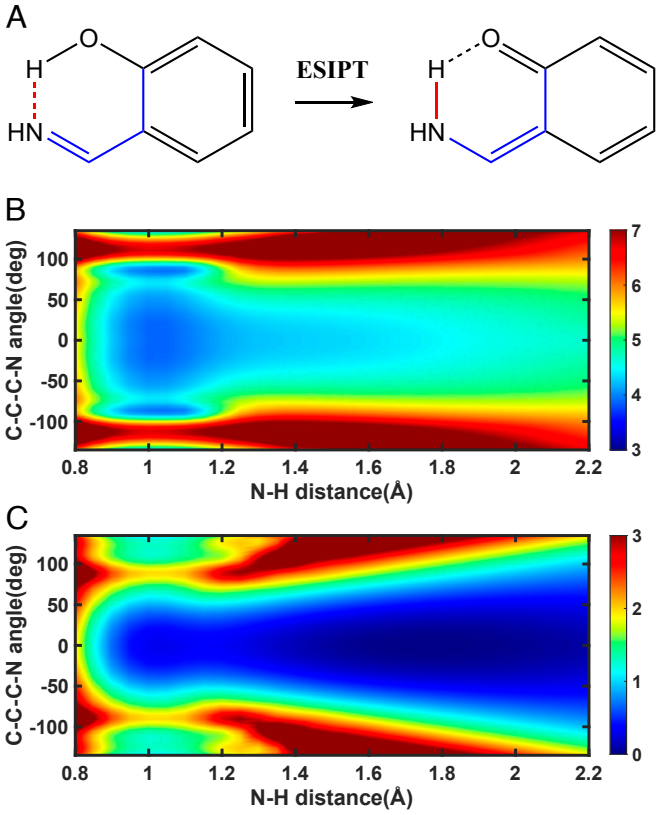

Fig. 1. (*A*) ESIPT in 2-(iminomethyl)phenol. The selected nuclear degrees of freedom are marked in red (N–H distance) and blue (C–C–C–N dihedral angle). (*B*) and (*C*) show the adiabatic potential energy surfaces of S_1 and S_0 in the two-dimensional nuclear space marked in (*A*). All energies are in eV.

Experimentally, ESIPT has been measured by time-resolved fluorescence and time-resolved photoelectron spectroscopy at valence levels (14, 18, 37, 38). These techniques are limited by their temporal resolution and by valence excited-state chemical shifts, which prohibit the detailed study of local dynamics. To overcome these challenges, we explore the unique features of TR-XPS to monitor ESIPT. The power of time-resolved X-ray absorption spectroscopies was recently demonstrated by a theoretical study of ESIPT (39) and by an experimental study of intermolecular proton transfer in solution (40).

In this work, we simulate the gas-phase TR-XPS signals in order to separately observe the local dynamics of both the proton donor and acceptor groups of the ESIPT process in 2-(iminomethyl)phenol. Schematic representation is sketched in Fig. 1*A*. This is a tautomerization from the *cis*-enol form to the *cis*-keto form. Potential energy surface calculations show that ESIPT in this case is barrierless, which leads to an ultrashort reaction. We show that by employing femtosecond X-ray pulses, both ultrafast hydrogen bond breaking and forming features can be observed with high temporal resolution. Large excited-state chemical shifts providing spectral information of ESIPT are predicted thanks to the high sensitivity of core ionization. We find that the site-selectivity of X-ray pulses can be used to identify the donor and acceptor groups of the proton transfer process. Through separate observation of the core level of the donor side and acceptor side, they can be clearly distinguished by their chemical shift dynamics. These features show significant advantages of TR-XPS compared to the simulated time-resolved photoelectron spectroscopy at the valence levels.

1. Quantum Dynamical Simulations

The ESIPT process of 2–(iminomethyl)phenol was studied in a reduced nuclear space of the N–H distance and the C–C–C–N dihedral angle (Fig. 1*A*). Since ESIPT typically happens within 30 fs, it is reasonable to only consider limited nuclear degrees of freedom. We note that an exact description of such a process would still require considering nuclear motions on multidimensional potential surfaces with all degrees of freedom taken into account. To partially include this effect, we performed a relaxed scan while constructing the potential energy surfaces (i.e., with geometry optimization at each individual geometry). Ground state (S_0) and exited state (S_1) electronic structure calculations were performed in Gaussian16 software (41) at density functional theory (DFT) and time-dependent density functional theory (TDDFT) level with M06-2X (42) functional and 6-311++G(d,p) basis set. The validity of this level of theory has been demonstrated in a previous study by comparison with high-level multiconfiguration methods (43). The adiabatic potential energy surfaces S_1 and S_0 are depicted in Fig. 1 *B* and *C*, respectively. At small C–C–C–N dihedral angles (−50° to 50°), with the N–H distance decreasing from ∼2 to ∼1 Å (from *cis*-enol form to *cis*-keto form), the S_0 energy surface gradually rises, indicating that spontaneous intramolecular proton transfer cannot happen in the ground state. In contrast, the S_1 energy surface monotonously goes down from the enol to the keto side as shown in Fig. 1*B*. The corresponding proton transfer is an ultrafast barrierless process.

We have performed exact nuclear wave packet dynamical simulations in the two-dimensional nuclear space by numerically solving the time-dependent Schrödinger equation. The pump excitation at $t = 0$ prepares the system to the S_1 energy surface. Initialized wake packet is localized in both the distance and dihedral angle dimensions. Fig. 2 shows the resulting in nuclear wave-packet dynamics at selected times t. As shown by the contour lines at 16.4 fs, the wave packet rapidly spreads along the N–H distance and reaches the intermediate area between the valence bond and hydrogen bond. At 26.6 fs, the wave packet arrives at the *cis*-keto side with the new N–H valence bond formed. It becomes more delocalized in both nuclear degrees of freedom. This emphasizes the need for a high temporal resolution techniques to observe the details of the ultrafast ESIPT process.

2. TR-XPS

TR-XPS signals were simulated aimed at monitoring the intramolecular proton transfer process. We consider a neutral molecule excited by the pump pulse at $t = 0$, and its subsequent electronic and nuclear dynamics probed by an ultrafast X-ray pulse at a variable time T which ionizes the molecule into cation and a photoelectron. The ultrafast probe pulse is given by $\boldsymbol{E}(t-T) = A\vec{\boldsymbol{e}}e^{-i\omega_X(t-T)}\mathcal{E}(t-T)$, with peak amplitude A, field polarization $\vec{\boldsymbol{e}}$, mean photon energy ω_X and envelope $\mathcal{E}(t)$ normalized to 1 at the maximum. The time-dependent wave function $|\Psi(\boldsymbol{q},t)\rangle = \sum_I |\chi_I(\boldsymbol{q},t)\rangle \otimes |\psi_I(\boldsymbol{q})\rangle$ describes the temporal evolution of the neutral molecule, where $|\chi_I(\boldsymbol{q},t)\rangle$ is the time-dependent wave packet on the Ith potential energy surface, $\{|\psi_I(\boldsymbol{q})\rangle\}$ is the adiabatic electronic states, and $\boldsymbol{q}$ is the two-dimensional vector of the nuclear coordinates in our model. The cation states created upon the photoionization are denoted by $\{|\phi_\alpha(\boldsymbol{q})\rangle\}$. Neglecting the Coulomb interaction between cation and photoelectron, the latter can be treated as free electron $H_{\text{free}} = \sum_{\boldsymbol{k}} \varepsilon_{\boldsymbol{k}} |\varphi_{\boldsymbol{k}}\rangle \langle\varphi_{\boldsymbol{k}}|$, where $\boldsymbol{k}$ runs over all the continuum states with kinetic energy $\varepsilon_{\boldsymbol{k}} = |\boldsymbol{k}|^2/2$. The

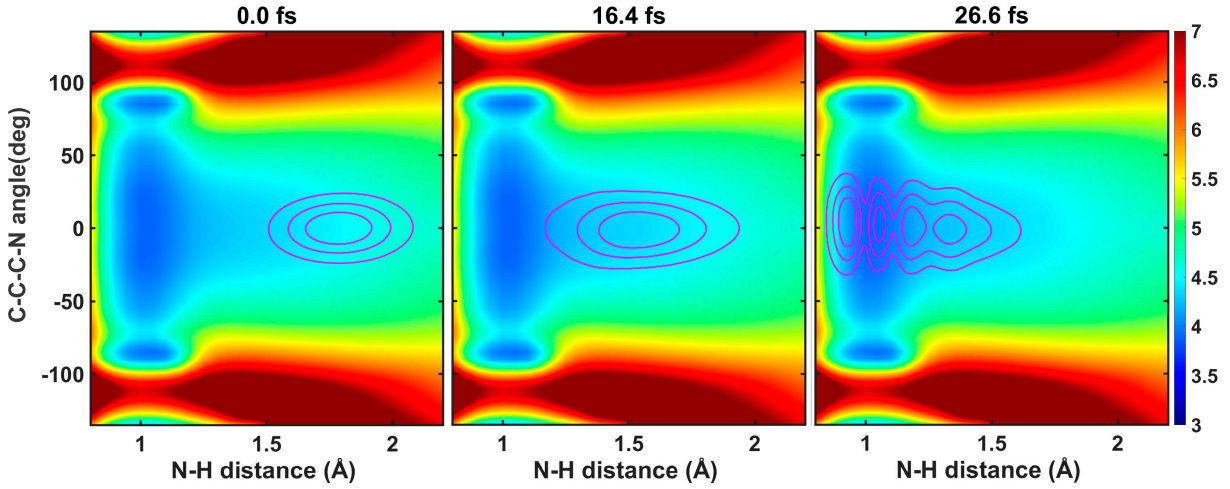

Fig. 2. Simulated nuclear wave packet dynamics in our two-dimensional nuclear space (N–H distance and C–C–C–N dihedral angle) at selected times t. Contour lines depict the nuclear wave-packet snapshots on the S_1 adiabatic potential energy surface. The potential energy (eV) is represented by the color intensity.

orientationally averaged TR-XPS signal, measured as a function of emitted photoelectron kinetic energy $\varepsilon_{\boldsymbol{k}}$ with probe pulse arrival time T was calculated by (25)

$$S^{\mathrm{TRXPS}}(\varepsilon_{\boldsymbol{k}}, T) = 2\mathcal{R}e \int_{-\infty}^{\infty} \mathrm{d}t \int_{0}^{\infty} \mathrm{d}t_1 \mathcal{E}^*(t-T) \times \mathcal{E}(t-t_1-T) \cdot e^{-i(\varepsilon_{\boldsymbol{k}}-\omega_X)t_1} \frac{\sqrt{2\varepsilon_{\boldsymbol{k}}}}{3} \times \sum_{II'\alpha i} \int d^2\boldsymbol{q} \int \mathrm{d}\Omega_{\varepsilon_{\boldsymbol{k}}} \chi^*_{I'}(\boldsymbol{q}, t) \vec{e}_i^* \cdot V_{I',\alpha\boldsymbol{k}}(\boldsymbol{q}) \times e^{-i\omega_\alpha t_1 - \Gamma t_1} \vec{e}_i \cdot V_{\alpha\boldsymbol{k},I}(\boldsymbol{q}) \chi_I(\boldsymbol{q}, t-t_1), \quad [1]$$

where the unit vector $\vec{e}_i$ runs over the three spatial directions x, y, and z. The natural linewidths Γ of oxygen (0.18 eV) and nitrogen (0.132 eV) 1s ionization are used (44). The calculation of transition dipole moments $\{V_{\alpha\boldsymbol{k},I}(\boldsymbol{q})\}$ is described in *Materials and Methods*. The key molecular properties needed for the spectroscopic simulation are the Dyson orbitals

$$\varphi^D_{\alpha I}(\boldsymbol{q}, \boldsymbol{r}) = \sqrt{N} \int d\boldsymbol{r}_2 \ldots \boldsymbol{r}_N \phi^*_\alpha(\boldsymbol{q}, \boldsymbol{r}_2 \ldots \boldsymbol{r}_N) \psi_I(\boldsymbol{q}, \boldsymbol{r}, \boldsymbol{r}_2 \ldots \boldsymbol{r}_N), \quad [2]$$

which are the overlaps between the N electron neutral molecule and $N-1$ electron cation system. The calculations were performed in NEWTONX software using TDDFT results of Gaussian16 (45).

The calculated Dyson orbitals at selected geometries corresponding to the oxygen 1s level, the nitrogen 1s level and the valence first ionization employed in our signal simulations are presented in Fig. 3. In Fig. 3 *A*–*C*, as the O–H distance is

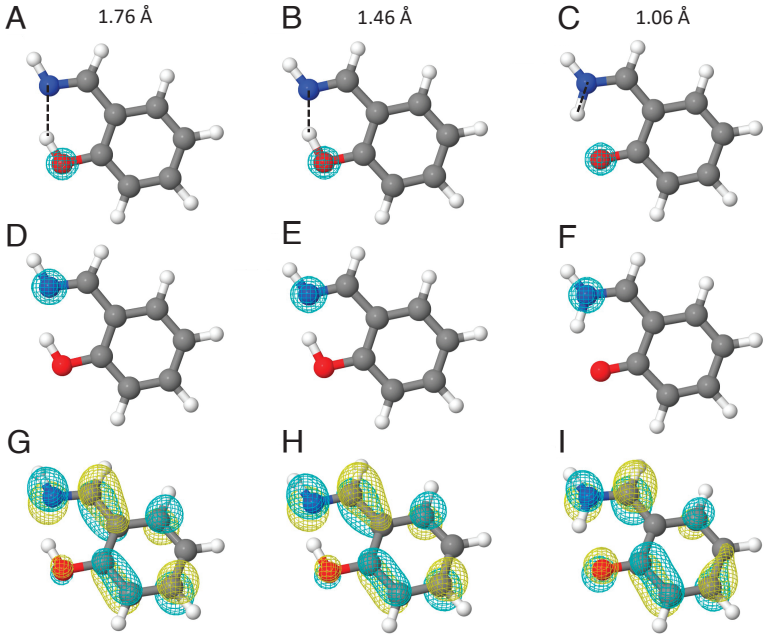

Fig. 3. (*A*–*C*) are Dyson orbitals of oxygen 1s ionization at N–H distances of 1.76 Å, 1.46 Å, and 1.06 Å, respectively. (*D*–*F*) same for the nitrogen 1s ionization. (*G*–*I*) same for the valence first ionization.The C–C–C–N dihedral angle are 0 for all geometries.

increased, the calculated oxygen 1s Dyson orbital remains localized around the donor oxygen atom of the proton transfer process. The nitrogen 1s Dyson orbital is also localized and centered on the acceptor nitrogen atom in panels *D*–*F*. For comparison, the valence Dyson orbitals of the first ionized cation state are presented in Fig. 3 *G*–*I*. The π type orbital is delocalized spanning the entire molecular system. Its shape only slightly changes from the enol form to the keto form. One should therefore not expect a prominent spectroscopic signature of ESIPT in this case due to the delocalized nature of valence ionization.

3. Results and Discussion

The simulated TR-XPS signals at the oxygen 1s and the nitrogen 1s levels are depicted in Fig. 4. We employed Gaussian X-ray ionization pulses with envelope $\mathcal{E}(t) = e^{-\frac{t^2}{(2\tau)^2}}$ and duration $\tau = 1$ fs. The time evolution of the average N–H distance and C–C–C–N dihedral angle along with their wave packet widths are also presented to show the explicit connection between nuclear motion and chemical shift. As shown by Fig. 4 *A* and *B*, the wave packet widths do not exhibit significant delocalization along the N–H distance and gradually increase in the C–C–C–N angle dimension during the proton transfer process. It becomes delocalized along the N–H distance but more local along the C–C–C–N angle at the end of the ESIPT. The intramolecular proton transfer process is clearly captured by the oxygen 1s signal in Fig. 4*C*. We notice a significant intensity decrease around 15 fs along with a rapid ionization energy red shift up to 2 eV. For comparison, chemical shifts of oxygen 1s ionization between enol and keto form of different molecules are around 2 to 4 eV as reported by static XPS experiments (46). The corresponding average N–H bond length decreases rapidly from ∼1.5 to ∼1.2 Å, indicating a intramolecular hydrogen bond is transforming into a valence bond. This reflects the intermediate state where the old O–H bond is breaking and the new N–H bond is forming. After 25 fs, the intensity above 535 eV decays and a new signal peak around 533.5 eV emerges, indicating that the proton transfer process is over. In Fig. 4*D*, the nitrogen 1s signal records this ultrafast process from the acceptor side. A similar intensity decrease can also be found at 15 fs. However, with the same intensity change, the acceptor nitrogen signal shifts to higher energies in contrast to the donor oxygen signal. The intensity below 400 eV decays after 25 fs and new peak emerges around 401 eV.

The observation of local dynamics by TR-XPS for intramolecular proton transfer is a notable result of the present study. We have demonstrated that the site-selectivity of X-ray pulses can be used to separately probe the donor and acceptor groups along the ESIPT process. Through separate measurements on the proton donor and acceptor atoms, the TR-XPS signal of the donor (oxygen) side has a considerable red shift and the acceptor (nitrogen) side signal exhibits blue shift. Even though femtosecond pulses can provide high temporal resolution for ultrafast dynamics, the associated spectral resolution cannot be generally guaranteed due to the weak selection rule of photoelectron spectroscopy. However, as shown by the simulated signals, the large energy shifts at the core-level ionization up to 2 eV make it possible to overcome the spectral broadening caused by ultrashort pulses. To further explore the optimal joint temporal and spectral resolution of TR-XPS, we calculated the oxygen 1s signals for probe pulses of 500 as and 200 as (Fig. 5 *A* and *B*). These attosecond pulses result in broadband signals up to several eVs, making it difficult to resolve the chemical shifts and intensity changing details of the ESIPT. Natural linewidth due to the short lifetime of core excited states is the other factor that may influence the spectral resolution. We also calculated the TR-XPS signals of the oxygen 1s and the nitrogen 1s ionization with the probe pulses approximated by delta functions in the frequency domain (very long pulses) to single out the spectral broadening effect of natural linewidth. As shown by Fig. 5 *C* and *D*, the corresponding signals are far narrower than the realistic signals in Fig. 4, indicating that its broadening is negligible and probe pulse broadening is dominant in the XPS signals. We demonstrated that one should choose suitable ultrashort pulses to achieve a balance between temporal and spectral resolution.

The large core exited-state chemical shifts and different shift directions observed in the signals are attributed to the electron charge dynamics of the donor and acceptor atom. ESIPT is a sigmatropic hydrogen shift reaction. From *cis*-enol form to the *cis*-keto product, the chemical bonding of the observed oxygen atom changes from C–O–H to C=O as illustrated in Fig. 1*A*, resulting in a carbon-oxygen bond order change. The atomic core orbitals are sensitive to their bonding configurations. In classical ESCA, core binding energies are determined by the electrostatic interaction of the core electron with the nucleus and the electrostatic shielding of the nuclear charge from all electrons in the atom (47). The latter can be altered by changes in chemical bonding of the atoms. From C–O–H to C=O groups, the core ionization energy of the donor oxygen decreased by

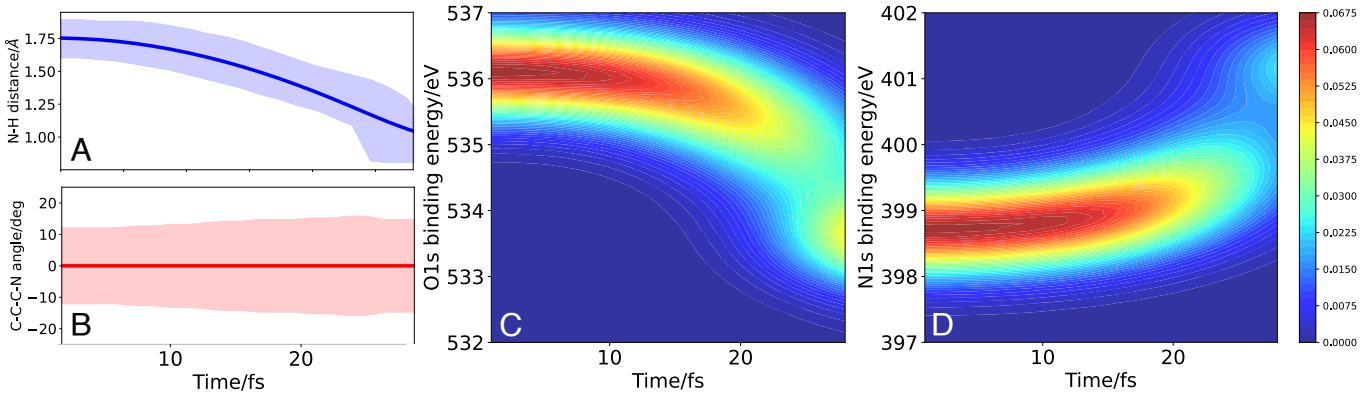

Fig. 4. (*A* and *B*) Time evolution of the average N–H distance and C–C–C–N dihedral angle calculated by the expectation value of wake packet. The corresponding wave packet widths represented by the full width at half maxima (FWHM) are also presented. (*C* and *D*) are TR-XPS signals for τ =1 fs probe pulses for the oxygen 1s ionization with mean photon energy 538 eV and the nitrogen 1s ionization 403 eV, respectively.

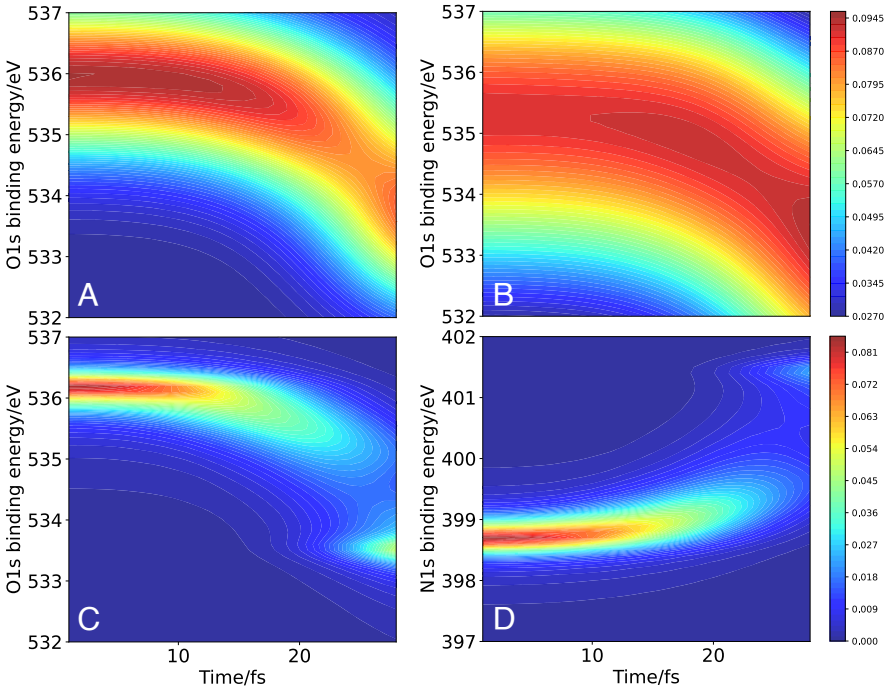

Fig. 5. (*A*) and (*B*) are TR-XPS signals for the oxygen 1s ionization with probe pulses of $\tau = 500$ as and 200 as, respectively. (*C*) and (*D*) are TR-XPS signals for the oxygen 1s ionization and the nitrogen 1s ionization calculated with probe pulses approximated by delta functions in the frequency domain, respectively.

more than 2 eV due to the addition of valence electron charge. On the acceptor side, the C=N–H group turns into C–NH_2 with a withdrawal of valence electron charge to the nitrogen atom. Hence the TR-XPS signal of the acceptor side shall have a positive ionization energy shift. The sensitivity of TR-XPS to atom-specific bonding situations makes it a potential tool of local reaction probe for not only proton transfer, but a wide range of ultrafast reactions involving local electron charge changes.

For comparison, the time-resolved photoelectron spectroscopy at the first valence ionization level of 2–(iminomethyl)phenol is simulated and presented in Fig. 6. The intensity change and chemical shift at 15 fs cannot be observed in the valence signal. Around 25 fs when the ESIPT has finished as shown in the previous TR-XPS signals, the only resolvable spectral signature is the increasing of signal peak. The bond-breaking details of the proton transfer process are missed in the calculated valence level photoelectron signal (Fig. 6) due to the delocalized nature of the valence ionization. As shown in Fig. 3 *G*–*I*, the Dyson orbitals employed to calculate the valence signals are π type orbitals spanning the entire molecule. The local details of the sigmatropic hydrogen shift in intramolecular proton transfer process therefore cannot be resolved by valence photoelectron spectroscopy. Note that we have only simulated the signals of the first ionization. In practice, due to the weak selection rule of photoelectron spectroscopy, different valence ionization signals may overlap, making the spectral resolution even worse. In contrast, the core ionization TR-XPS exhibits high temporal resolution and shows rapid excited-state chemical shifts. The site-selectivity of X-ray pulses allows distinctive observation of the proton transfer details from both the donor and acceptor sides. The unique features obtained by TR-XPS for monitoring ESIPT ultrafast dynamics are revealed.

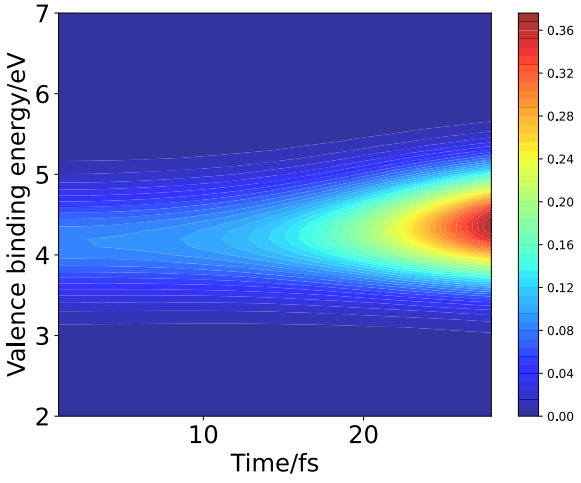

Fig. 6. Time-resolved photoelectron signals at the first valence ionization level of 2–(iminomethyl)phenol for 1 fs probe pulse.

4. Conclusions

We have simulated the gas-phase TR-XPS signals that monitor the ESIPT of 2-(iminomethyl)phenol. Individual core ionization probes of both the proton donor oxygen atom and acceptor nitrogen atom were studied. Chemical bond breaking and forming details of the molecule undergoing intramolecular hydrogen bond exchanging are captured. Significant intensity change and rapid red shift of ionization energies are observed in the TR-XPS signal of the donor oxygen atom. The TR-XPS signal of the acceptor nitrogen atom, in contrast, shows a rapid blue shift during the proton transfer process. The proton donor and acceptor groups can be therefore distinguished by separately probing their local dynamics. Thanks to the large chemical shifts of core ionization, high spectral resolution can be obtained despite the lack of selection rules in photoelectron spectroscopy.

We would like to mention the connection and complementary relation of TR-XPS and ultrafast X-ray and electron diffraction techniques (48–53). Femtosecond X-ray and electron diffraction

are capable of imaging all the molecular motions as opposed to local motions. There are limits in spatial resolution in diffraction experiments and details of local changes in charge redistribution of key small groups can be complemented by TR-XPS. A joint study of these two techniques may provide a more profound understanding of chemical reactions with global spatial observation and local energetic features.

We have demonstrated the sensitivity of TR-XPS signals for local chemical environments of the probed atoms in molecules. The different spectral features of proton donor and acceptor atoms stem from the associated valence bond-order changes. The time evolution of the chemical shifts in TR-XPS can provide a unique access to local bonding dynamics of different kinds of ultrafast chemical processes.

5. Materials and Methods

5.1. Simulation of the Wave Packet Dynamics. The wave packet is initialized on the S_1 surface using Franck–Condon approximation. Arnoldi propagation with a time step of 0.024 fs is employed. Potential energy surfaces and related molecular quantities in this two-dimensional space are calculated with ab initio quantum chemistry and subsequently discretized on a numerical grid with 128 grid points in the N–H distance and 512 grid points in the C–C–C–N dihedral angle.

5.2. Calculation of the Transition Dipole Moment. Using the orthogonality between cation and free electrons, the transition dipole moment can be approximately calculated by (54)

$$V_{\alpha \boldsymbol{k},I}(\boldsymbol{q}) = \langle \phi_\alpha(\boldsymbol{q}) \otimes \varphi_{\boldsymbol{k}}(\boldsymbol{q}) | \hat{V} | \psi_I(\boldsymbol{q}) \rangle \approx \int d\boldsymbol{r} \frac{e^{i\boldsymbol{k}\boldsymbol{r}} \cdot \boldsymbol{r}}{\sqrt{8\pi^3}} \varphi^D_{\alpha I}(\boldsymbol{q}, \boldsymbol{r}), \quad [3]$$

where $\hat{V}$ is the dipole operator and $\{\varphi^D_{\alpha I}(\boldsymbol{q}, \boldsymbol{r})\}$ are Dyson orbitals.

Data, Materials, and Software Availability. All study data are included in the article and/or *SI Appendix*.

ACKNOWLEDGMENTS. This work was primarily supported by the U.S. Department of Energy, Office of Science, Office of Basic Energy Sciences, grant. FG02-04ER15571. Y.G., H.Y., and B.G. were supported by NSF grant CHE-2246379. These grants are gratefully acknowledged. S.M. is a senior fellow of the Hagler Institute of Advanced Study at Texas A&M University.

Author affiliations: [a]Department of Chemistry, University of California, Irvine, CA 92697-2025; [b]Department of Physics and Astronomy, University of California, Irvine, CA 92697-2025; [c]Department of Chemistry and Biochemistry, University of California, San Diego, La Jolla, CA 92093; and [d]Department of Chemistry, Westlake University, Hangzhou, Zhejiang 310030, China

1. M. Paddock, S. Rongey, G. Feher, M. Okamura, Pathway of proton transfer in bacterial reaction centers: Replacement of glutamic acid 212 in the l subunit by glutamine inhibits quinone (secondary acceptor) turnover. *Proc. Natl. Acad. Sci. U.S.A.* **86**, 6602–6606 (1989).
2. F. Garczarek, K. Gerwert, Functional waters in intraprotein proton transfer monitored by FTIR difference spectroscopy. *Nature* **439**, 109–112 (2006).
3. M. Rini, B. Z. Magnes, E. Pines, E. T. Nibbering, Real-time observation of bimodal proton transfer in acid-base pairs in water. *Science* **301**, 349–352 (2003).
4. O. F. Mohammed, D. Pines, J. Dreyer, E. Pines, E. T. Nibbering, Sequential proton transfer through water bridges in acid-base reactions. *Science* **310**, 83–86 (2005).
5. S. J. Formosinho, L. G. Arnaut, Excited-state proton transfer reactions. II. Intramolecular reactions. *J. Photochem. Photobiol. A Chem.* **75**, 21–48 (1993).
6. A. Douhal, F. Lahmani, A. H. Zewail, Proton-transfer reaction dynamics. *Chem. Rev.* **207**, 477–498 (1996).
7. S. J. Lim, J. Seo, S. Y. Park, Photochromic switching of excited-state intramolecular proton-transfer (ESIPT) fluorescence: A unique route to high-contrast memory switching and nondestructive readout. *J. Am. Chem. Soc.* **128**, 14542–14547 (2006).
8. A. C. Sedgwick *et al*., Excited-state intramolecular proton-transfer (ESIPT) based fluorescence sensors and imaging agents. *Chem. Soc. Rev.* **47**, 8842–8880 (2018).
9. H. Gu *et al*., Excited-state intramolecular proton transfer (ESIPT) based fluorescent probes for biomarker detection: Design, mechanism, and application. *Chem. Commun.* **59**, 2056–2071 (2023).
10. L. Chen *et al*., Ultrafast water sensing and thermal imaging by a metal-organic framework with switchable luminescence. *Nat. Commun.* **8**, 15985 (2017).
11. V. Misra, H. Mishra, Photoinduced proton transfer coupled with energy transfer: Mechanism of sensitized luminescence of terbium ion by salicylic acid doped in polymer. *J. Chem. Phys.* **128**, 244701 (2008).
12. M. Smoluch, H. Joshi, A. Gerssen, C. Gooijer, G. van der Zwan, Fast excited-state intramolecular proton transfer and subnanosecond dynamic stokes shift of time-resolved fluorescence spectra of the 5-methoxysalicylic acid/diethyl ether complex. *J. Phys. Chem. A* **109**, 535–541 (2005).
13. E. A. E. H. Abou El, A. Fujii, T. Ebata, N. Mikami, Substitution effects on the excited-state intramolecular proton transfer of salicylic acid: An infrared spectroscopic study on the oh stretching vibrations of jet-cooled 5-methoxysalicylic acid. *Chem. Phys. Lett.* **376**, 788–793 (2003).
14. S. Lochbrunner *et al*., Dynamics of excited-state proton transfer systems via time-resolved photoelectron spectroscopy. *J. Chem. Phys.* **114**, 2519–2522 (2001).
15. S. Lochbrunner, K. Stock, E. Riedle, Direct observation of the nuclear motion during ultrafast intramolecular proton transfer. *J. Mater. Chem.* **700**, 13–18 (2004).
16. S. Takeuchi, T. Tahara, Coherent nuclear wavepacket motions in ultrafast excited-state intramolecular proton transfer: Sub-30-fs resolved pump–probe absorption spectroscopy of 10-hydroxybenzo[H]quinoline in solution. *J. Phys. Chem. A* **109**, 10199–10207 (2005).
17. J. Herek, S. Pedersen, L. Banares, A. Zewail, Femtosecond real-time probing of reactions. IX. Hydrogen-atom transfer. *J. Chem. Phys.* **97**, 9046–9061 (1992).
18. T. Sekikawa, O. Schalk, G. Wu, A. E. Boguslavskiy, A. Stolow, Initial processes of proton transfer in salicylideneaniline studied by time-resolved photoelectron spectroscopy. *J. Phys. Chem. A* **117**, 2971–2979 (2013).
19. B. Gu, S. Sun, F. Chen, S. Mukamel, Photoelectron spectroscopy with entangled photons; enhanced spectrotemporal resolution. *Proc. Natl. Acad. Sci. U.S.A.* **120**, e2300541120 (2023).
20. F. Krausz, M. Ivanov, Attosecond physics. *Rev. Mod. Phys.* **81**, 163 (2009).
21. C. Pellegrini, A. Marinelli, S. Reiche, The physics of X-ray free-electron lasers. *Rev. Mod. Phys.* **88**, 015006 (2016).
22. J. Duris *et al*., Tunable isolated attosecond X-ray pulses with gigawatt peak power from a free-electron laser. *Nat. Photonics* **14**, 30–36 (2020).
23. P. Maroju *et al*., Attosecond pulse shaping using a seeded free-electron laser. *Nature* **578**, 386–391 (2020).
24. K. Bennett, M. Kowalewski, S. Mukamel, Nonadiabatic dynamics may be probed through electronic coherence in time-resolved photoelectron spectroscopy. *J. Chem. Theory Comput.* **12**, 740–752 (2016).
25. S. M. Cavaletto, D. Keefer, S. Mukamel, Electronic coherences in nonadiabatic molecular photophysics revealed by time-resolved photoelectron spectroscopy. *Proc. Natl. Acad. Sci. U.S.A.* **119**, e2121383119 (2022).
26. S. P. Neville, M. Chergui, A. Stolow, M. S. Schuurman, Ultrafast X-ray spectroscopy of conical intersections. *Phys. Rev. Lett.* **120**, 243001 (2018).
27. L. Inhester, Z. Li, X. Zhu, N. Medvedev, T. J. Wolf, Spectroscopic signature of chemical bond dissociation revealed by calculated core-electron spectra. *J. Phys. Chem. Lett.* **10**, 6536–6544 (2019).
28. M. L. Vidal, A. I. Krylov, S. Coriani, Dyson orbitals within the fc-CVS-EOM-CCSD framework: Theory and application to X-ray photoelectron spectroscopy of ground and excited states. *Phys. Chem. Chem. Phys.* **22**, 2693–2703 (2020).
29. K. R. Siefermann *et al*., Atomic-scale perspective of ultrafast charge transfer at a dye-semiconductor interface. *J. Phys. Chem. Lett.* **5**, 2753–2759 (2014).
30. F. Brauße *et al*., Time-resolved inner-shell photoelectron spectroscopy: From a bound molecule to an isolated atom. *Phys. Rev. A* **97**, 043429 (2018).
31. T. Leitner *et al*., Time-resolved electron spectroscopy for chemical analysis of photodissociation: Photoelectron spectra of $Fe(CO)_5$, $Fe(CO)_4$, and $Fe(CO)_3$. *J. Chem. Phys.* **149**, 044307 (2018).
32. S. Pathak *et al*., Tracking the ultraviolet-induced photochemistry of thiophenone during and after ultrafast ring opening. *Nat. Chem.* **12**, 795–800 (2020).
33. R. Santra, N. V. Kryzhevoi, L. S. Cederbaum, X-ray two-photon photoelectron spectroscopy: A theoretical study of inner-shell spectra of the organic para-aminophenol molecule. *Phys. Rev. Lett.* **103**, 013002 (2009).
34. K. M. G. Siegbahn, A discussion on photoelectron spectroscopy–electron spectroscopy for chemical analysis (ESCA). *Philos. Trans., Math. Phys.* **268**, 33–57 (1970).
35. I. Gabalski *et al*., Time-resolved X-ray photoelectron spectroscopy: Ultrafast dynamics in CS_2 probed at the S 2p edge. *J. Phys. Chem. Lett.* **14**, 7126–7133 (2023).
36. D. Mayer *et al*., Following excited-state chemical shifts in molecular ultrafast X-ray photoelectron spectroscopy. *Nat. Commun.* **13**, 198 (2022).
37. S. Ameer-Beg *et al*., Ultrafast measurements of excited state intramolecular proton transfer (ESIPT) in room temperature solutions of 3-hydroxyflavone and derivatives. *J. Phys. Chem. A* **105**, 3709–3718 (2001).
38. P. Wnuk *et al*., From ultrafast events to equilibrium-uncovering the unusual dynamics of ESIPT reaction: The case of dually fluorescent diethyl-2,5-(dibenzoxazolyl)-hydroquinone. *Phys. Chem. Chem. Phys.* **16**, 2542–2552 (2014).
39. C. M. Loe, C. Liekhus-Schmaltz, N. Govind, M. Khalil, Spectral signatures of ultrafast excited-state intramolecular proton transfer from computational multi-edge transient X-ray absorption spectroscopy. *J. Phys. Chem. Lett.* **12**, 9840–9847 (2021).
40. Z. Yin *et al*., Femtosecond proton transfer in urea solutions probed by X-ray spectroscopy. *Nature* **619**, 749–754 (2023).
41. M. J. Frisch *et al*., *Gaussian 16 Revision A 03* (Gaussian Inc., Wallingford, CT, 2016).
42. Y. Zhao, D. G. Truhlar, The M06 suite of density functionals for main group thermochemistry, thermochemical kinetics, noncovalent interactions, excited states, and transition elements: Two new functionals and systematic testing of four M06-class functionals and 12 other functionals. *Theor. Chem. Acc.* **120**, 215–241 (2008).
43. J. Kim, D. Kim, Theoretical investigation of excited-state intramolecular proton transfer and photoisomerization of 2-(iminomethyl) phenol. *J. Phys. Chem. A* **123**, 7246–7254 (2019).
44. J. Campbell, T. Papp, Widths of the atomic K-N7 levels. *At. Data Nucl. Data Tables* **77**, 1–56 (2001).

45. M. Barbatti *et al*., Newton-X: A surface-hopping program for nonadiabatic molecular dynamics. *WIREs Comput. Mol. Sci.* **4**, 26–33 (2014).
46. R. Brown, A. Tse, T. Nakashima, R. Haddon, Symmetries of hydrogen-bonded enol forms of diketones as determined by X-ray photoelectron spectroscopy. *J. Am. Chem. Soc.* **101**, 3157–3162 (1979).
47. U. Gelius, Recent progress in ESCA studies of gases. *J. Electron Spectrosc. Relat. Phenom.* **5**, 985–1057 (1974).
48. T. J. Wolf *et al*., The photochemical ring-opening of 1,3-cyclohexadiene imaged by ultrafast electron diffraction. *Nat. Chem.* **11**, 504–509 (2019).
49. H. Yong *et al*., Determination of excited state molecular structures from time-resolved gas-phase X-ray scattering. *Faraday Discuss.* **228**, 104–122 (2021).
50. H. Yong *et al*., Ultrafast X-ray scattering offers a structural view of excited-state charge transfer. *Proc. Natl. Acad. Sci. U.S.A.* **118**, e2021714118 (2021).
51. E. G. Champenois *et al*., Femtosecond electronic and hydrogen structural dynamics in ammonia imaged with ultrafast electron diffraction. *Phys. Rev. Lett.* **131**, 143001 (2023).
52. M. Centurion, T. J. Wolf, J. Yang, Ultrafast imaging of molecules with electron diffraction. *Annu. Rev. Phys. Chem.* **73**, 21–42 (2022).
53. A. A. Ischenko, P. M. Weber, R. D. Miller, Capturing chemistry in action with electrons: Realization of atomically resolved reaction dynamics. *Chem. Rev.* **117**, 11066–11124 (2017).
54. S. Sun, D. B. Williams-Young, T. F. Stetina, X. Li, Generalized Hartree–Fock with nonperturbative treatment of strong magnetic fields: Application to molecular spin phase transitions. *J. Chem. Theory Comput.* **15**, 348–356 (2018).

Supporting information of Chemical Bond Reorganization in Intramolecular Proton Transfer Revealed by Ultrafast X-ray Photoelectron Spectroscopy

Yonghao Gu,[*,†] Haiwang Yong,[*,‡] Bing Gu,[¶] and Shaul Mukamel[*,†]

†*Department of Chemistry and Department of Physics and Astronomy, University of California, Irvine, California 92697-2025, United States*

‡*Department of Chemistry and Biochemistry, University of California San Diego, La Jolla, California, 92093, United States*

¶*Department of Chemistry, Westlake University, Hangzhou, Zhejiang 310030, China*

E-mail: yonghaog@uci.edu; hyong@ucsd.edu; smukamel@uci.edu

Electronic structure calculations of 2-(iminomethyl)phenol

The initial molecular geometry was optimized at the neutral ground state using DFT with the M06-2X[1] functional at a basis set level of 6-311++G(d,p). Cation excited states were calculated with linear response TDDFT using the same functional and basis set. All computations were performed with Gaussian 16 software.[2] The optimized neutral ground state geometry is presented in Table S1.

Table S1: ground state optimized geometry of 2-(iminomethyl)phenol

Atom	x/Å	y/Å	z/Å
C	2.291198	-0.166613	0.000000
C	1.380526	0.872795	0.000000
C	0.000000	0.631030	0.000000
C	-0.467528	-0.701191	0.000000
C	0.458064	-1.750066	0.000000
C	1.815154	-1.481764	0.000000
H	3.354797	0.032837	0.000000
H	1.726285	1.901916	0.000000
H	0.078735	-2.764299	0.000000
H	2.517674	-2.307235	0.000000
O	-1.768522	-1.004604	0.000000
H	-2.283475	-0.164323	0.000000
C	-0.928301	1.756621	0.000000
H	-0.467424	2.750251	0.000000
N	-2.195166	1.593107	0.000000
H	-2.706936	2.471058	0.000000

Wavepacket dynamics of 2-(iminomethyl)phenol excited-state intramolecular proton transfer

We have performed exact nuclear wave packet dynamical simulations in the two-dimensional nuclear space (N-H distance and C-C-C-N dihedral angle) by numerically solving the time-dependent Schrödinger equation. The simulated wavepacket dynamics at selected times t are presented in Figure S1.

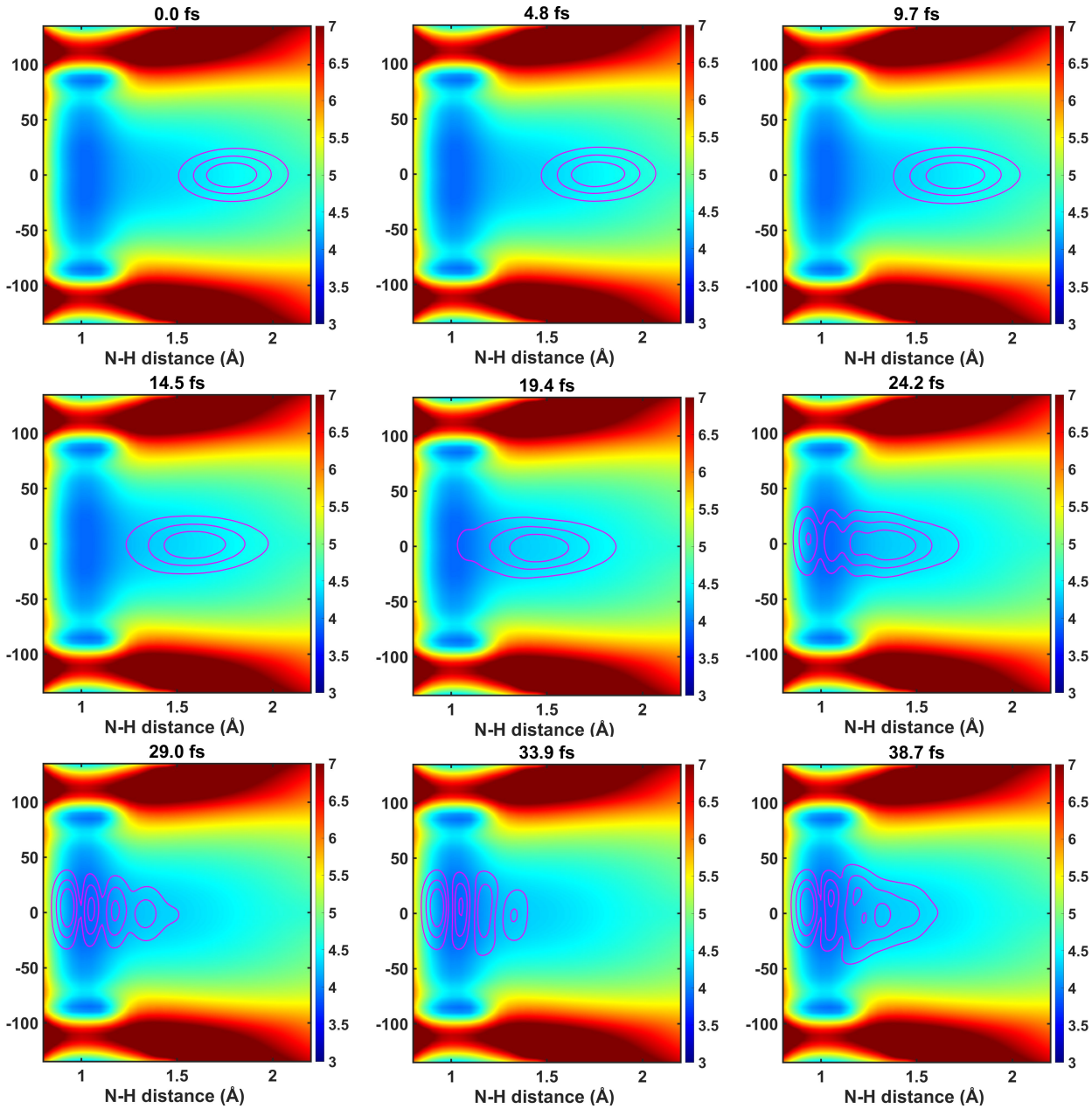

Figure S1: Simulated nuclear wave packet dynamics in our two-dimensional nuclear space (N-H distance and C-C-C-N dihedral angle) at selected times t. Contour lines depict the nuclear wave-packet snapshots on the S_1 adiabatic potential energy surface. The potential energy (eV) is represented by the color intensity.

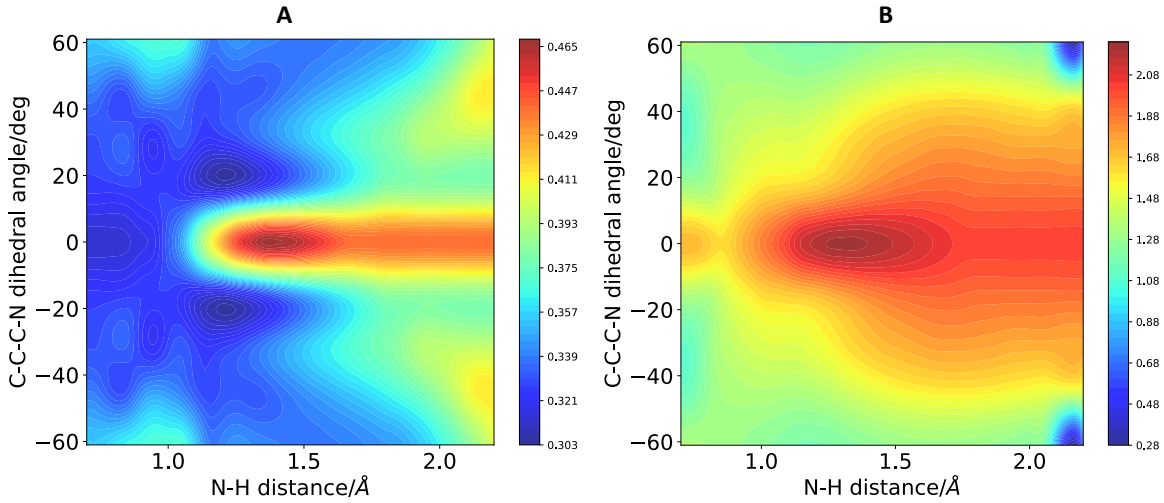

Figure S2: Photoelectron cross sections of oxygen 1s (A) and nitrogen 1s (B) ionization. The probe pulses are 538 eV and 403 eV as for oxygen and nitrogen, respectively.

Cross sections of XPS for the O1s and N1s core ionization

The photoelectron cross sections σ of oxygen 1s and nitrogen 1s ionization in the N-H distance and CCCN dihedral angle space are calculated and presented in Figure S2. They are calculated by[3]

$$\sigma(k, \omega_X) = \int d\Omega_{\epsilon_{\boldsymbol{k}}} \frac{4\pi^2 k \omega_X}{c} \left| V_{\alpha \boldsymbol{k}, I}(\boldsymbol{q}) \right|^2 \tag{1}$$

where the photoelectron kinetic energy $\epsilon_{\boldsymbol{k}}$ is 1 eV and probe pulses ω_X are 538 eV (oxygen) and 403 eV (nitrogen).

References

(1) Zhao, Y.; Truhlar, D. G. The M06 suite of density functionals for main group thermochemistry, thermochemical kinetics, noncovalent interactions, excited states, and transition elements: two new functionals and systematic testing of four M06-class functionals and 12 other functionals. *Theor. Chem. Acc.* **2008**, *120*, 215–241.

(2) Frisch, M. J. et al. Gaussian 16 RevisionA 03. Gaussian, Inc.: Wallingford, CT, 2016.

(3) Reed, K. J.; Zimmerman, A. H.; Andersen, H. C.; Brauman, J. I. Cross sections for photodetachment of electrons from negative ions near threshold. *J. Chem. Phys.* **1976**, *64*, 1368–1375.